

Verification of High-Resolution RAMS Forecasts over East-Central Florida during the 1999 and 2000 Summer Months

JONATHAN L. CASE, JOHN MANOBIANCO, ALLAN V. DIANIC, AND MARK M. WHEELER

ENSCO, Inc., Cocoa Beach, and Applied Meteorology Unit, NASA, Kennedy Space Center, Florida

DEWEY E. HARMS

45th Weather Squadron, U.S. Air Force, Patrick Air Force Base, Florida

CARLTON R. PARKS

ACTA, Inc., Cape Canaveral, and 45th Space Wing/Eastern Range Safety, Patrick Air Force Base, Florida

(Manuscript received 31 January 2002, in final form 4 June 2002)

ABSTRACT

This paper presents an objective and subjective verification of a high-resolution configuration of the Regional Atmospheric Modeling System (RAMS) over east-central Florida during the 1999 and 2000 summer months. Centered on the Cape Canaveral Air Force Station (CCAFS), the innermost nested grid of RAMS has a horizontal grid spacing of 1.25 km, thereby providing forecasts capable of modeling finescale phenomena such as ocean and river breezes, and convection. The RAMS is run operationally at CCAFS within the Eastern Range Dispersion Assessment System (ERDAS), in order to provide emergency response guidance during space operations. ERDAS uses RAMS wind and temperature fields for input into ERDAS diffusion algorithms; therefore, the accuracy of dispersion predictions is highly dependent on the accuracy of RAMS forecasts. The most substantial error in RAMS over east-central Florida is a surface-based cold temperature bias, primarily during the daylight hours. At the Shuttle Landing Facility, the RAMS point error statistics are not substantially different than the National Centers for Environment Prediction Eta Model; however, an objective evaluation consisting of only point error statistics cannot adequately determine the added value of a high-resolution model configuration. Thus, results from a subjective evaluation of the RAMS forecast sea breeze and thunderstorm initiation on the 1.25-km grid are also presented. According to the subjective verification of the Florida east coast sea breeze, the RAMS categorical and skill scores exceeded that of the Eta Model predictions in most instances. The RAMS skill scores in predicting thunderstorm initiation are much lower than the sea-breeze evaluation scores, likely resulting from the lack of a sophisticated data assimilation scheme in the current operational configuration.

1. Introduction

The Regional Atmospheric Modeling System (RAMS; Pielke et al. 1992) numerical weather prediction (NWP) model is run in real time at the Cape Canaveral Air Force Station (CCAFS) to support operations of the U.S. space program. RAMS represents the NWP portion of the Eastern Range Dispersion Assessment System (ERDAS; Lyons et al. 1993), which was developed by the Mission Research Corporation (MRC)/ASTER Division for the U.S. Air Force (USAF). Delivered to the Eastern Range at CCAFS in March 1994, ERDAS was designed to provide emergency response guidance for the 45th Space Wing/Eastern Range Safety (45 SW/SE) operations at the Kennedy Space Center

(KSC) and CCAFS in the event of a hazardous material release or an aborted vehicle launch. The prognostic gridded data from RAMS are available to ERDAS for display and input to the Hybrid Particle and Concentration Transport (HYPACT) model (Walko et al. 2001). The HYPACT model provides three-dimensional dispersion predictions using RAMS forecast grids to represent the environmental conditions.

An evaluation of the prototype ERDAS was conducted during the period from March 1994 to December 1995 by the Applied Meteorology Unit (AMU), an organization operated jointly under a triagency memorandum of understanding by the National Aeronautics and Space Administration (NASA), the USAF, and the National Weather Service (Ernst and Merceret 1995). The AMU evaluation (Evans 1996) concluded that ERDAS provided significant enhancement over existing toxic dispersion modeling capabilities at CCAFS. The report also offered a number of recommendations for further

Corresponding author address: Jonathan L. Case, ENSCO, Inc., 1980 N. Atlantic Ave., Suite 230, Cocoa Beach, FL 32931.
E-mail: case.jonathan@ensco.com

improvements to the RAMS configuration. These recommendations were implemented in the next generation of ERDAS, which also contains an upgraded version of RAMS.

There are two significant differences between the original and upgraded versions of the RAMS configuration in ERDAS. First, the original configuration of RAMS ran without cloud microphysics whereas the current, upgraded configuration is run with mixed-phase cloud microphysics. Second, the areal extent of the innermost forecast grid over east-central Florida was expanded and the horizontal grid spacing was reduced from 3.00 to 1.25 km.

The RAMS evaluation primarily concentrates on wind, temperature, and stability forecasts that are required for dispersion predictions using the HYPACT model. Since RAMS forecast data provide input to the HYPACT model, the accuracy of dispersion predictions is highly dependent upon the accuracy of RAMS forecasts. As a result, the primary goal of the evaluation is to determine the accuracy of RAMS forecasts during all seasons and under various weather regimes over east-central Florida. For brevity, this paper focuses only on the model evaluation during the 1999 and 2000 summer months, since operationally significant, local-scale weather phenomena occur most frequently in central Florida during the summer.

Some recent studies have evaluated RAMS at high resolutions for specific applications, primarily utilizing objective point error statistics. Snook et al. (1998) and Powell and Rinard (1998) presented the local configuration and point error statistics for 8- and 2-km RAMS forecasts over the southeastern United States in support of weather forecasts for the 1996 centennial Olympic Games. McQueen et al. (1997) evaluated RAMS forecasts over the Chesapeake Bay against buoy observations for air pollution applications. Snook et al. (1995) described an operational configuration of the Local Analysis and Prediction System (LAPS) and RAMS at 10-km horizontal grid spacing, which was designed to run in a local weather office on an inexpensive workstation.

This paper provides a summary of the AMU's evaluation of the upgraded RAMS configuration in ERDAS for the 1999 and 2000 Florida warm seasons, focusing on local results at KSC/CCAFS and the immediate surrounding region. The comprehensive warm- and cool-season evaluations from 1999 and 2000 can be found in Case (2000, 2001). The RAMS evaluation is divided into two segments, an objective component and a subjective component. The objective component focuses on model point error statistics at a number of observational locations. Since point error statistics cannot adequately evaluate meteorological phenomena and mesoscale patterns such as sea breezes and precipitation, there is also a subjective portion of the evaluation. The subjective component involves the examination of forecasts and

observations to determine how RAMS predicts such phenomena over east-central Florida.

The remaining portion of the paper is organized as follows. Section 2 describes the real-time configuration of RAMS as run operationally within ERDAS. Section 3 explains the objective and subjective methodologies used in the RAMS verification. The results of the objective verification for the 1999 and 2000 Florida warm seasons are presented in section 4. This section also includes a classification of RAMS errors according to various weather regimes, a comparison between the operational configuration and a coarser-grid configuration of RAMS, and a benchmark of RAMS versus the Eta Model at the Space Shuttle Landing Facility (three-letter identifier TTS). Section 5 summarizes the results of the subjective evaluation focusing on the verification of the sea breeze during the 1999 and 2000 warm seasons, and thunderstorm initiation during the 2000 warm season. Section 6 summarizes the paper.

2. Real-time RAMS configuration at CCAFS

a. RAMS configuration in ERDAS

In the operational ERDAS configuration, the three-dimensional, nonhydrostatic mode of RAMS (version 4a) is run on four nested grids with a horizontal grid spacing of 60, 15, 5, and 1.25 km (Fig. 1). RAMS uses a stretched vertical coordinate from near the surface up to 18.195 km, with additional vertical levels in grids 3 and 4 to provide enhanced vertical resolution near the ground. A summary of the horizontal and vertical grid parameters is provided in Table 1. The physical parameterization schemes used in ERDAS RAMS include a microphysics scheme following Cotton et al. (1982), a modified Kuo cumulus convection scheme (Tremback 1990), the Chen and Cotton (1988) radiation scheme, a Mellor and Yamada (1982)-type turbulence closure, and an 11-layer soil-vegetation model (Tremback and Kessler 1985) with fixed soil moisture in the initial condition. The modified Kuo scheme is run on grids 1-3 whereas grid 4 utilizes explicit convection only. The mixed-phase microphysics scheme is run on all four grids.

b. RAMS forecast cycle

RAMS is initialized twice daily at 0000 and 1200 UTC using the Eta 12-h forecast grids from its forecast cycle 12 h earlier (because of operational time constraints), as well as available observational data including the CCAFS rawinsonde (XMR), aviation routine weather reports (METAR), buoys, and KSC/CCAFS wind tower, and 915-MHz and 50-MHz Doppler Radar Wind Profiler (DRWP) data. No variational data assimilation or nudging technique is applied when incorporating observational data. Instead, RAMS is initialized from a cold start by integrating the model forward in

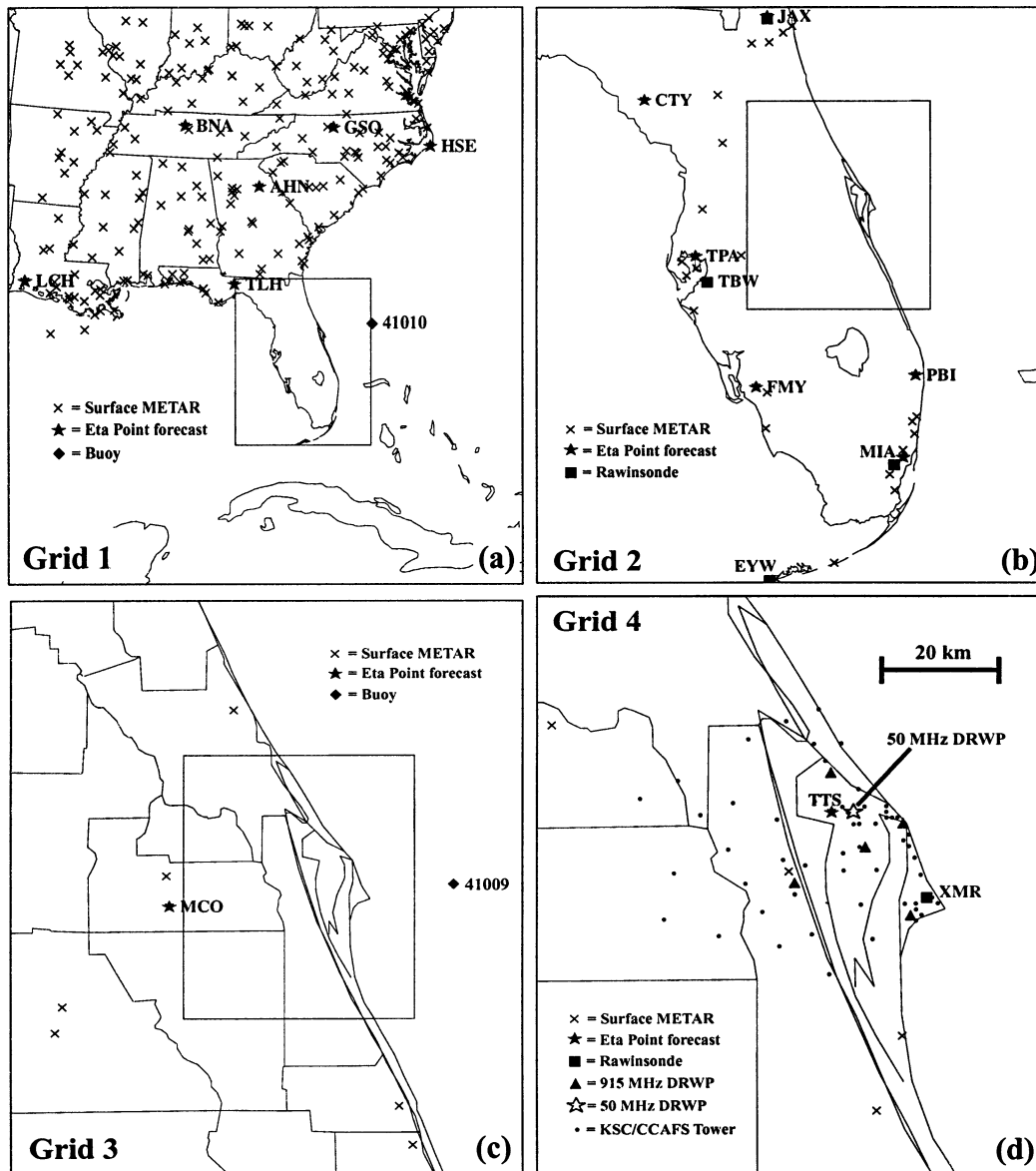


FIG. 1. A display of the surface and upper-air stations used for point verification of RAMS on all four forecast grids. RAMS point forecasts are verified in the highest-resolution grid within which each station is located; thus, stations are only shown in the grid in which they are verified. The observational data used for verification include surface METAR stations (X), buoys (filled diamond), rawinsondes (filled square), KSC/CCAFS 915-MHz DRWP [filled triangles in (d)], the KSC/CCAFS 50-MHz DRWP [open star in (d)], and Eta point forecast locations (filled star). The locations of the inner nested grid within its parent grid is shown in (a), (b), and (c).

time from a gridded field without any balancing or data assimilation steps. Observational data are analyzed onto hybrid coordinates using the RAMS Isentropic Analysis (ISAN) package (Tremback 1990). The ISAN hybrid coordinate consists of a combination of isentropes and terrain-following surfaces on which data are analyzed within the RAMS model domain, similar to the National Centers for Environmental Prediction (NCEP) Rapid Update Cycle model (Benjamin et al. 1998). For sea surface temperature initialization, RAMS uses fixed monthly climatological means on grid 1, and these val-

ues are subsequently interpolated to the inner grids. The lateral boundary conditions are nudged (Davies 1983) by 12–36-h forecasts from the NCEP Eta Model, interpolated onto an 80-km grid. Output from the Eta Model is available every 6 h for boundary conditions to RAMS. Two-way interactive boundary conditions are used on the inner three nested grids.

The RAMS cycle is run in real time for a 24-h forecast period on a Hewlett-Packard (HP) K460 workstation consisting of 12 processors. The model run-time performance is optimized by using a message passing in-

TABLE 1. A summary of the grid configuration parameters for all four RAMS grids. The model parameters include the number of grid points in the x , y , and z directions (n_x , n_y , and n_z), horizontal grid spacing (dx), minimum and maximum vertical resolutions (dz_{min} and dz_{max}), and the heights of the minimum and maximum physical vertical levels (z_{-min} and z_{-max}), with all distances given in meters.

Grid	n_x	n_y	n_z	dx	dz_{min}	dz_{max}	z_{-min}^*	z_{-max}
1	36	40	33	60 000	50	750	23	18 195
2	38	46	33	15 000	50	750	23	18 195
3	41	50	36	5000	25	750	11	18 195
4	74	90	36	1250	25	750	11	18 195

* Here, z_{-min} actually represents the second vertical level above ground. For computational purposes, the height of the first model level for each grid is below ground at -20 , -20 , -11 , and -11 m for grids 1, 2, 3, and 4, respectively.

terface (MPI) on the 12 processors. In MPI, the runtime is significantly reduced in comparison with a single processor because each processor simultaneously performs computations on a portion of the domain (Tremback et al. 1998). The operational cycle requires approximately 15 min to analyze observational data for the initial conditions using ISAN and 10–12 h to complete the 24-h forecast cycle. On occasions when the model produced extensive convection (primarily during the summer months), a 24-h forecast could not be completed in 12 h because of the calculations associated with the microphysics scheme. In these instances, the existing RAMS run is terminated before the 24-h simulation is completed, and the new simulation begins. Consequently, RAMS data are occasionally missing from the 22–24-h forecasts when extensive model convection occurs. It is important to note, however, that all forecast hours preceding the premature cycle termination are used when computing error statistics for this evaluation, thereby precluding any possible bias in the results. In the event of a one-cycle failure, prognostic data are still available from the previous forecast cycle, providing overlap between successive 0000 or 1200 UTC runs.

RAMS forecast output is available once per hour for display and analysis purposes because of disk-space limitations of the operational hardware. Thus, all portions of this model verification study are limited in time to a frequency of 1 h, regardless of the frequency of available observational data. It is important to note that warm-season weather phenomena in Florida can develop over timescales shorter than 1 h (particularly convection). Nonetheless, hourly forecast output at high spatial resolution has the potential to provide valuable guidance in forecasting warm-season phenomena in east-central Florida.

3. Evaluation methodology

The evaluation of RAMS during the 1999 and 2000 warm seasons includes both an objective and a subjective component. The objective component is designed

to present a representative set of model errors of winds, temperature, and moisture for both the surface and the upper levels. The goal of the subjective verification is to provide an assessment of the forecast timing and propagation of the central Florida east coast sea breeze (ECSB) and forecast thunderstorm initiation by examining selected RAMS forecast fields.

a. Objective evaluation

The objective component of the RAMS evaluation presented in this paper consists of three separate segments of point error statistics. First, a verification of the operational four-grid configuration of RAMS was conducted for daily forecasts from May to August 1999 and May to September 2000. Second, a surface wind regime classification and thunderstorm-day regime classification were performed for daily forecasts during the 2000 summer months. Third, the RAMS errors were compared with the Eta Model errors at TTS for the 2000 warm season.

In all instances, point forecasts were extracted from RAMS grids using the RAMS/HYPACT Evaluation and Visualization Utilities (REVVU) software Tremback et al. (2002). By specifying the latitude, longitude, and sensor height for each observational location, REVVU interpolates forecast data in three dimensions from surrounding RAMS grid points using the grid with the finest horizontal resolution. For sensor heights below the first model physical level, REVVU vertically interpolates between the belowground computational level and the first physical level above ground rather than performing similarity theory calculations.

1) STANDARD FOUR-GRID EVALUATION

The standard objective evaluation consists of point forecast error statistics for the operational RAMS configuration during the 1999 and 2000 Florida warm seasons. The 0–24-h point forecasts of wind, temperature, and moisture were compared with data from surface METAR and buoy stations, the XMR rawinsonde, the KSC/CCAFS wind towers, five 915-MHz and one 50-MHz DRWP at all available observational locations on grid 4, and selected surface and rawinsonde stations on grids 1–3. Throughout the course of this study, RAMS was verified at all of these observational sensors on grids 1–4; however, this paper focuses primarily on error statistics at sensors located in the 1.25-km forecast grid because of the local interests of east-central Florida forecasters. Specifically, the verification sensors include the KSC/CCAFS wind-tower network, the XMR rawinsonde, the buoys offshore of CCAFS, and the TTS surface station.

The point statistics computed include the root-mean-square (rms) error, bias (forecast – observed), and error standard deviation (SD) of wind direction, wind speed, temperature, and dewpoint. The error SD was computed

TABLE 2. The number of days during the 2000 warm season experiencing surface winds classified as onshore (easterly component), offshore (westerly component), or light and variable. Wind speeds less than 2.6 m s^{-1} (5 kt) were classified as light. The regime was classified according to the winds around 1200 UTC at the 16.5-m (54 ft) level of the KSC/CCAFS towers.

RAMS cycle	Onshore	Offshore	Light
0000 UTC	44	53	33
1200 UTC	50	61	35

using the Murphy (1988) decomposition for rms error. In addition, the mean values of forecasts and observations for these variables were computed as a function of forecast hour at all observational sites for the entire evaluation period. Special care was exercised when computing the mean and SD of wind direction errors following Turner (1986). However, in general, the mean observed and forecast wind direction quantities have little meaning because their distributions were nearly uniform. Therefore, only plots of rms error and bias are discussed for wind direction. In this evaluation, we have generally assumed that the magnitude of the observational error is negligible when compared with the model error.

For purposes of interpretation, the total error (rms error) includes contributions from both systematic and random errors. Systematic error (bias) can be caused by a consistent misrepresentation of physical parameters such as radiation or model convection. Nonsystematic or random errors, given by the error SD, are caused by uncertainties in the model initial condition or unresolvable differences in scales between the forecasts and observations (Nutter and Manobianco 1999). Note that the error SD also contains a component of natural observed variability since the model value is an average over a grid volume, whereas the observed value is a discrete, point measurement.

A quality control (QC) check was performed on all point error statistics to remove any errors greater than three standard deviations from the mean error. The QC check was performed to remove bad observations or individual corrupted model point forecasts, typically caused by input/output problems. This QC generally resulted in the rejection of less than 2% of all possible error pairs.

2) REGIME CLASSIFICATION FOR 2000 WARM SEASON

The second segment of the objective evaluation involves the computation of point error statistics under various weather regimes for the operational RAMS configuration during the 2000 warm season only. Specifically, two types of regimes are examined in this paper, surface winds and thunderstorm days. During each day, the surface wind regime was identified according to the early morning wind flow (~ 1200 UTC) observed at the

TABLE 3. A contingency table of the daily occurrence of 1200 UTC RAMS predicted vs observed thunderstorms on grid 4 for all successful forecasts during the 2000 FL warm season.

1200 UTC forecast cycle	Observed thunderstorms	No observed thunderstorms
Forecast thunderstorms	72	25
No forecast thunderstorms	11	38

16.5-m level of the KSC/CCAFS wind tower network. The days were then grouped into three classes of wind flow patterns: offshore, onshore, and light, where light winds were defined as sustained speeds less than 2.6 m s^{-1} (5 kt). The RAMS forecasts were grouped together according to these surface wind flows (Table 2), and error statistics were compiled for the RAMS forecasts under each wind regime. The total number of 1200 UTC forecasts is slightly larger than the 0000 UTC forecasts in Table 2 because the 1200 UTC RAMS cycle contained fewer forecast cycle failures during the 2000 warm season. Thus, we only present wind regime classification results from the 1200 UTC cycle in this paper.

For the thunderstorm regime classification, the occurrence of both observed and forecast thunderstorms were recorded during each day of the 2000 warm season for both forecast cycles. Observed thunderstorm days were identified by the occurrence of cloud-to-ground lightning [from the Cloud-to-Ground Lightning Surveillance System (CGLSS; Harms et al. 1997) in central Florida] on grid 4 at any time from 1500 to 2300 UTC. RAMS forecast thunderstorm days were identified using the empirical technique described in section 3. Every day was categorized according to the occurrence of observed and forecast thunderstorms within the area of grid 4. (The data and functionality for classifying observed and forecast thunderstorms were developed just prior to the 2000 warm season and, thus, were not available for the 1999 warm season.) Each RAMS forecast fell into one of four categories as shown in the contingency table for the 1200 UTC forecast cycle (Table 3). Subsequently, the RAMS errors at the KSC/CCAFS wind towers were computed for each of the four possible combinations of observed versus forecast thunderstorm days. Again, only thunderstorm regime results from the 1200 UTC cycle are presented in this paper.

3) BENCHMARK OF RAMS VERSUS 32-KM ETA AT TTS

The third segment of the objective evaluation consists of a benchmark of RAMS versus the 32-km version of the Eta Model point forecasts at TTS. This benchmark compares RAMS forecasts to the NCEP Eta Model and quantifies any added value that may be provided by RAMS over the Eta Model, based on an objective comparison. It is important to note that since the Eta grids were not archived for interpolation to individual station locations, the Eta point forecast products provided by

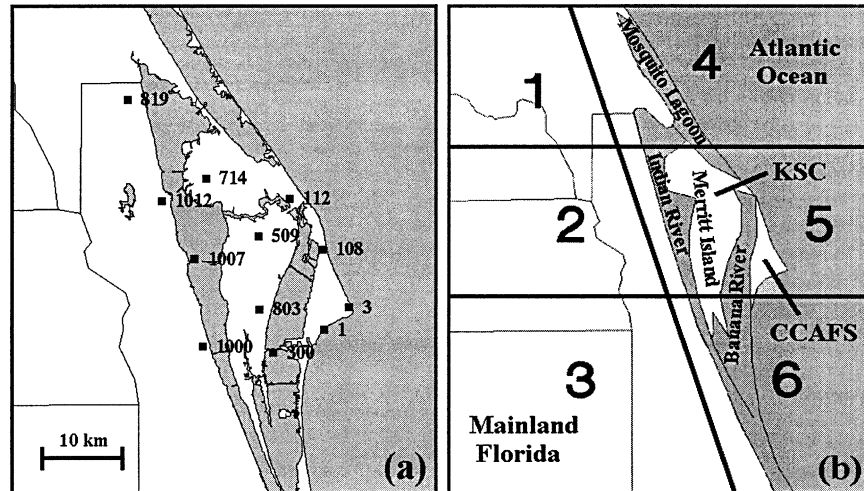


FIG. 2. (a) A plot of the 12 KSC/CCAFS wind towers used in the subjective sea-breeze evaluation. (b) The six-zone classification scheme used for the warm-season subjective precipitation verification during the months of May–Sep 2000. The division between the western (1–3) and eastern zones (4–6) is designed to parallel the east-central FL east coast. The locations of significant land and water geographical features are noted.

NCEP were utilized instead (Chuang and Manikin 2002). As a result, this paper focuses on the RAMS–Eta comparison at TTS (surface only), since this station is the only available Eta point forecast location within RAMS grid 4.

b. Subjective evaluation during 1999 and 2000 warm seasons

A purely objective evaluation cannot adequately assess the potential strengths of a high-resolution model configuration. Small spatial and temporal errors in mesoscale phenomena can lead to unrepresentative error statistics in the objective evaluation. Therefore, the RAMS evaluation supplements the objective statistics with a subjective evaluation, in which the forecast fields and plots are manually examined and verified for various meteorological phenomena such as sea breezes and thunderstorms. This section outlines the subjective methodology used to verify RAMS forecast sea breezes and thunderstorm initiation during the 1999 and 2000 summer months.

1) 1999–2000 SEA-BREEZE VERIFICATION

The sea-breeze verification was conducted at 12 selected KSC/CCAFS wind towers across east-central Florida (Fig. 2a). All archived RAMS forecasts from May–August 1999 and May–September 2000 were examined to verify the forecast sea breeze. Point forecasts were generated at each wind tower site by interpolating in three dimensions the gridded RAMS forecasts from the innermost 1.25-km grid to the exact sensor height and location. These point forecasts and observations were examined at the 12 selected KSC/CCAFS wind

towers, representing three different zones of east-central Florida (the coastal barrier islands, Merritt Island, and mainland Florida). In each zone, four towers were identified in a north–south orientation that contained the most data for both the 1999 and 2000 Florida warm seasons. Twelve-panel graphical plots displaying both the forecast and observed wind direction and speed were generated for all RAMS forecast cycles to verify the occurrence and timing of the sea breeze at each selected wind tower.

Both *Geostationary Operational Environmental Satellite-8 (GOES-8)* visible imagery and Weather Surveillance Radar, model 74C, reflectivity data were used to identify the occurrence of the sea breeze on a given day. A sea-breeze front along Florida’s east coast is typically accompanied by a sharp clearing line and reflectivity fine-line that propagate westward with time. To determine the occurrence and timing of the sea-breeze passage, each KSC/CCAFS wind tower was examined for the development and maintenance of a wind shift to an onshore wind component (wind direction between 335° and 155° , the approximate orientation of the Florida east coast). The definition of an onshore versus offshore wind at coastal towers 1 and 3 varied from the rest of the towers because of the specific orientation of the coastline along the tip of Cape Canaveral (Fig. 2a). At these towers, onshore flow was defined as a wind direction between 335° (NW) and 180° (S) at tower 1 and between 335° (NW) and 200° (SSW) at tower 3. As a result, both of these towers have a larger range of onshore wind directions compared to the other towers. During easterly flow regimes, a sea-breeze passage was determined by a distinct increase in the negative (easterly) u wind at each wind tower. These same wind criteria were then applied to the RAMS forecasts

interpolated to each wind tower location to determine the forecast sea-breeze passage. The occurrence of a forecast and observed sea breeze was verified on a per tower basis in order to incorporate a spatial verification of the phenomenon.

In addition to the evaluation of the RAMS-predicted ECSB at the 12 selected towers, two benchmark-sensitivity tests were conducted as part of the sea-breeze verification. The first sensitivity study compares the RAMS four-grid sea-breeze forecasts to RAMS three-grid forecasts, where grid 4 is simply excluded and the model is rerun for all days with only the outer three grids. The sea-breeze verification is conducted at the same 12 wind towers for all common four- and three-grid RAMS forecasts only during the 2000 warm season. The second sensitivity experiment compares the RAMS four-grid sea-breeze forecasts with the Eta point forecasts at TTS. The TTS sea-breeze verification was performed for all common RAMS and Eta point forecasts during the 1999 and 2000 warm seasons. The same on-shore versus offshore criterion as used for the KSC/CCAFS wind tower evaluation was applied when verifying the RAMS and Eta sea-breeze forecasts at TTS.

A 2×2 contingency table was used to summarize the verification statistics based on the occurrence of both an observed and forecast sea breeze at any of the 12 KSC/CCAFS towers. A "hit" was defined as the occurrence of both an observed and a forecast sea-breeze passage at a particular KSC/CCAFS tower. Because RAMS forecast output is available once per hour, the timing of the onset and movement of the sea-breeze front was verified to the nearest hour at each of the 12 KSC/CCAFS towers.

From the contingency table, categorical and skill scores were calculated following Schaefer (1990) and Doswell et al. (1990). These scores include the bias, probability of detection (POD), false alarm rate (FAR), critical success index (CSI), and the Heidke skill score (HSS). In a perfect forecast, the bias, POD, CSI, and HSS are equal to unity and the FAR is 0. Note that the contingency table bias described here has a desired value of unity, different than the bias of the point forecasts, which has a desired value of 0. The timing error statistics were computed for all forecast hits. Both the rms error and bias (in hours) were calculated for the timing errors.

2) THUNDERSTORM INITIATION VERIFICATION (SUMMER 2000)

A technique was developed to identify the first observed and forecast thunderstorm to the nearest hour on RAMS grid 4 following Manobianco and Nutter (1999). Grid 4 was divided into six separate zones, three coastal and three inland (Fig. 2b). Forecast and observed data were examined between the hours of 1500 and 2300 UTC daily from 1 May to 30 September 2000. This validation time window was chosen for four reasons. First, warm-season thunderstorms occur most frequently

in central Florida during these hours (Reap 1994). In addition, both the 0000 and 1200 UTC RAMS forecast cycles from the same day overlap this time frame. Third, NWP models that are cold-started, such as the RAMS configuration in this study, require a "spinup" time period (roughly a few hours) before the model can generate precipitation adequately (Mohanty et al. 1986; Takano and Segami 1993). Last, the climatological distribution of diurnal lightning over the east coast of Florida during the summer months increases dramatically after 1500 UTC (Lericos et al. 2002, their Fig. 4).

Archived CGLSS data and GOES-8 visible imagery were used to identify the first observed thunderstorm in each zone of RAMS grid 4 on an hourly basis. Since NWP models such as RAMS do not explicitly predict lightning and thunderstorms, an empirical technique was adopted to define a model-predicted thunderstorm. Applying results from an east-central Florida dual-Doppler observational study conducted during the Convection and Precipitation/Electrification Experiment (Yuter and Houze 1995a,b), a model thunderstorm was defined by a predicted vertical velocity of 2 m s^{-1} or greater at 7-km height in conjunction with a forecast precipitation rate of at least 5 mm h^{-1} (0.2 in h^{-1}). This definition ensures that the model convection and updraft have reached a height where mixed-phase water particles co-exist, a condition found in electrified clouds (Bringi et al. 1997).

In traditional threat score methods, precipitation is verified at each individual grid point for various intensity thresholds, not accounting for small displacement errors that may occur in the model. In this subjective verification, the thunderstorm initiation is verified within each grid-4 zone rather than at each grid point. Furthermore, instead of determining the skill at different intensities, the definition of a model thunderstorm is fixed and applied to a varying time verification window. For each day that RAMS correctly predicted the occurrence of a thunderstorm within the grid-4 domain, the spatial and timing accuracy of thunderstorm initiation were examined by developing contingency tables, and determining categorical and skill scores for each individual grid-4 zone based on specific timing thresholds of 1, 2, and 3 h. Thus, a contingency table was developed separately for each grid-4 zone to verify the predicted thunderstorm initiation to within 1, 2, and 3 h of the first observed daily thunderstorm. To prevent possible biases in the results, only days with successful runs of both the 0000 and 1200 UTC forecast cycles were used to compile the contingency tables.

4. Objective verification results

a. 1999 and 2000 warm-season months

1) SURFACE

The most prominent error in RAMS during the 1999 and 2000 summers was a surface-based, primarily daytime

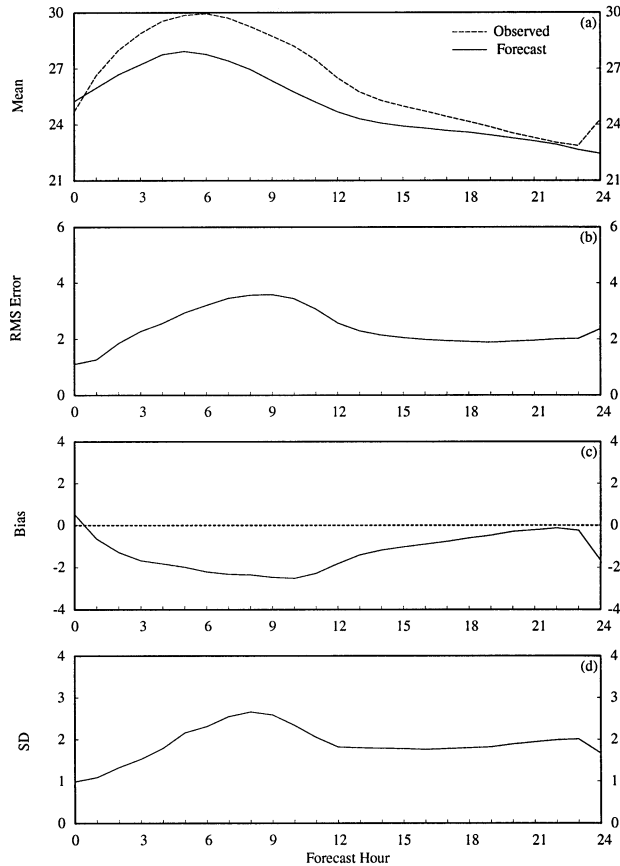


FIG. 3. Temperature errors ($^{\circ}\text{C}$) from the 1200 UTC operational RAMS forecast cycle during the 1999 and 2000 warm seasons, verified at the 1.8-m level of the KSC/CCAFS wind tower network (station locations in Fig. 1). Parameters plotted as a function of forecast hour are (a) mean observed (dashed) and forecast temperatures (solid), (b) rms error, (c) bias, and (d) error standard deviation (SD).

cold temperature bias at all observational sensors on grids 3 and 4. Figures 3 and 4 summarize the evolution of the 1200 UTC RAMS surface temperature errors over the KSC/CCAFS wind towers and the two buoys offshore of CCAFS, respectively. The rms error at the KSC/CCAFS wind towers peaks at about 3.5°C during the 8–9-h forecasts (Fig. 3b), whereas the cold bias exceeding -2°C peaks at 10 h (Fig. 3c). At the offshore buoys, the rms error and cold bias steadily increase from 1 to 7 h, then remain nearly constant thereafter (Figs. 4a and 4b). Because the random temperature error is proportional to the diurnal temperature variation (which is very small at the buoys), the error SD is nearly constant at only 1°C during all 24 forecast hours (not shown).

This cold bias is consistent with the results found in Snook et al. (1998), who reported cold daytime temperature biases during real-time RAMS simulations over the southeastern United States in support of the 1996 summer Olympic Games. Their sensitivity experiments suggested that RAMS was slow in mixing out the

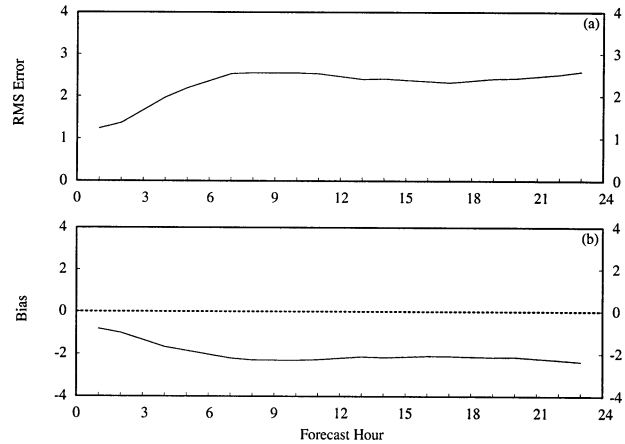


FIG. 4. Temperature errors ($^{\circ}\text{C}$) from the 1200 UTC operational RAMS forecast cycle during the 1999 and 2000 warm seasons, verified at the two buoys offshore of central FL (station locations in Fig. 1). Parameters plotted as a function of forecast hour are (a) rms error and (b) bias.

boundary layer during the late morning hours. In contrast, a recent study by Salvador et al. (1999) showed a warm daytime temperature bias in RAMS simulations at two coastal locations in Spain. By running several experiments to isolate the possible cause of this cold bias over central Florida, the AMU found that RAMS tended to develop widespread fog near the surface over both the land and water, resulting in delayed heating over the land during the morning hours. However, at buoy locations over the western Atlantic Ocean, this excessive fog does not explain the presence of a cold bias over water. A verification of the RAMS climatological SST data at buoy 41009 (see Fig. 1c) during the 2000 summer months indicates that the SST field was adequately represented, since the magnitude of the SST bias (ranging from -0.4° to $+0.8^{\circ}\text{C}$, not shown) is small when compared with the surface temperature bias ($\sim -2.0^{\circ}$ to -2.5°C). From these limited experiments, the AMU was unable to isolate the process(es) that caused the development of excessive fog in the version of RAMS run at CCAFS. Additional detailed testing with RAMS was beyond the scope of the current study.

The RAMS surface dewpoint errors exhibit a small dry bias at the KSC/CCAFS wind towers (not shown). The model consistently has about a -1°C dry bias at nearly all forecast hours. Meanwhile, the rms error and SD grow only about 1°C from 0 to 6 h, then maintain a constant error thereafter (not shown).

The RAMS forecast wind speeds at the KSC/CCAFS contain a $1\text{--}2\text{ m s}^{-1}$ positive bias, primarily during the afternoon and evening hours (4–15 h in Fig. 5b). Since the ECSB typically propagates westward through the KSC/CCAFS tower network during the late morning and early afternoon hours (1500–1800 UTC; Cetola 1997), these results suggest that the forecast wind speeds are slightly too strong following the passage of the ECSB. The rms error grows steadily to 7 h, and then

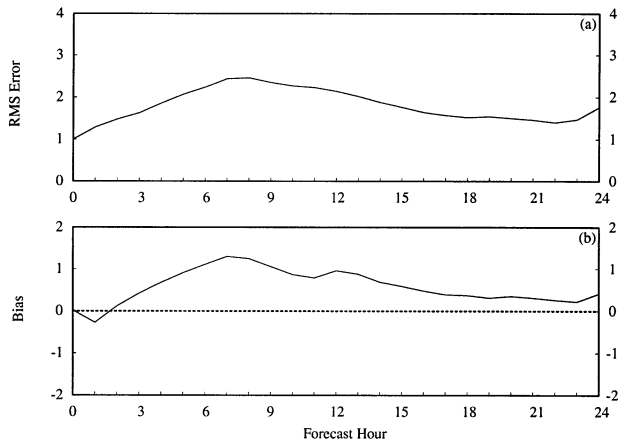


FIG. 5. Wind speed errors (m s^{-1}) from the 1200 UTC operational RAMS forecast cycle during the 1999 and 2000 warm seasons, verified at the 16.5-m level of the KSC/CCAFS wind tower network (station locations in Fig. 1). Parameters plotted as a function of forecast hour are (a) rms error and (b) bias.

decreases thereafter (Fig. 5a). At the two offshore buoys, the rms error and SD are nearly constant at 2 m s^{-1} during all 24 forecast hours with virtually no bias prevalent (not shown).

The wind direction errors at the KSC/CCAFS towers are given in Fig. 6 and show a rapid increase in rms error from 20° to 40° between initialization and the 1-h forecast. After 1 h, the rms error remains at or slightly above 40° through 18 h (0600 UTC), after which the rms errors again increase to about 60° to 65° (Fig. 6a). This peak in surface wind direction rms error occurs during the light and variable wind regime of the late night and early morning hours, possibly caused by an inability of RAMS to predict adequately the return flow associated with nocturnal land breezes. With a magnitude of less than 10° , the wind direction bias is negligible relative to the total error, suggesting mostly a random error component (Fig. 6b). However, the u -wind component experiences a $1\text{--}2 \text{ m s}^{-1}$ easterly bias during the afternoon and evening hours, corresponding to the times of the mean post-sea-breeze regime (not shown).

2) UPPER LEVELS

The upper-level temperature errors at XMR are characterized by a lower-tropospheric cold bias. The forecasts at 3, 10, and 22 h all show that RAMS predicts a temperature profile that is too stable relative to observations (Fig. 7). The main contributor to the overly stable forecast profile is a substantial cool bias below 650 mb that steadily increases to a maximum at the surface. The rms error also increases from 650 mb down to the surface; however, with the exception of the surface, the SD of the errors is nearly constant at about 1°C as a function of height for all three forecast times (not shown). Thus, the primary contributor to the growth

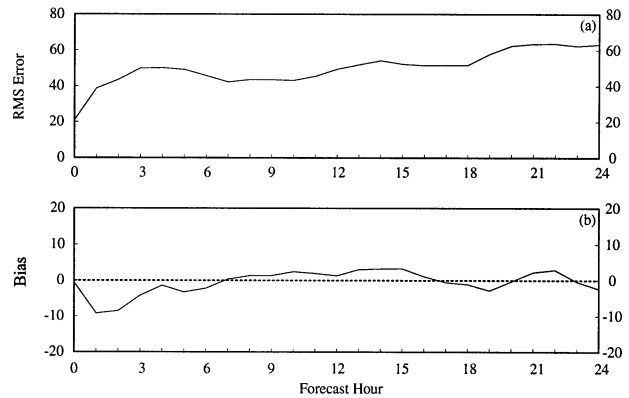


FIG. 6. Wind direction errors ($^\circ$) from the 1200 UTC operational RAMS forecast cycle during the 1999 and 2000 warm seasons, verified at the 16.5-m level of the KSC/CCAFS wind tower network (station locations in Fig. 1). Parameters plotted as a function of forecast hour are (a) rms error and (b) bias.

of the rms error in the lower troposphere is the model's cold bias.

The wind direction errors verified at XMR in the lowest 100 mb indicate that RAMS forecasts have the largest errors near the surface for the 3- and 22-h forecasts (1500 and 1000 UTC, respectively, shown in Fig. 8). At these times, the rms error decreases with height from the surface to about 950 mb. Meanwhile, the wind direction errors during the late-afternoon, post-sea-breeze regime (10 h) have a somewhat different profile between

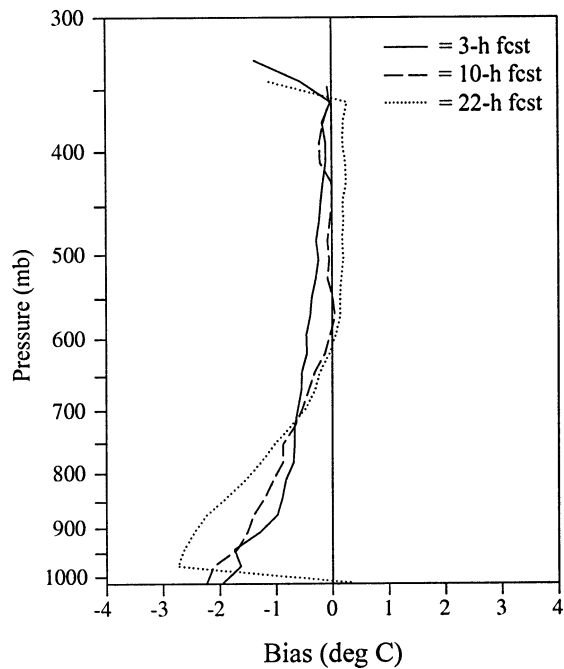


FIG. 7. Vertical profile of the RAMS temperature bias ($^\circ\text{C}$) at XMR from the 1200 UTC forecast cycle during the 1999 and 2000 warm seasons. The valid forecast times are 3, 10, and 22 h according to the scale provided.

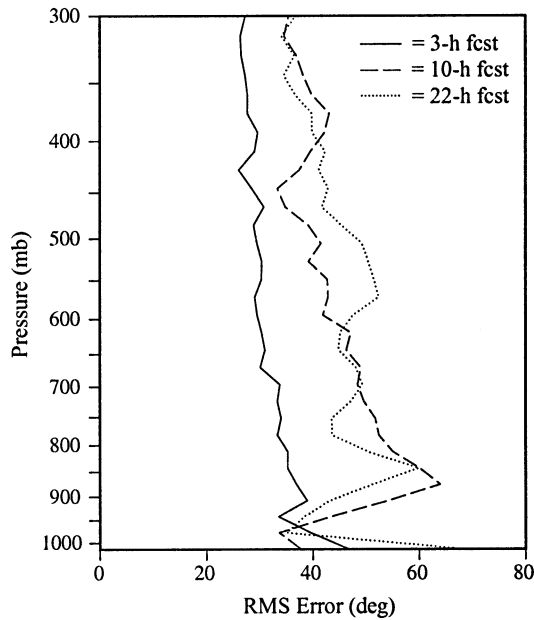


FIG. 8. Vertical profiles of wind direction rms errors ($^{\circ}$) at XMR from the 1200 UTC operational RAMS forecast cycle during the 1999 and 2000 warm seasons. The valid forecast times are 3, 10, and 22 h according to the scale provided.

the surface and 800 mb. During the mean post-sea-breeze regime, the wind direction rms errors increase from about 35° near the surface to over 60° at 875 mb. This late-afternoon error structure could result from consistently accurate predictions of the sea-breeze onset and propagation near the surface (refer to the results of the east coast sea-breeze subjective verification in section 5a), combined with uncertainty in the depth of the sea-breeze circulation. Meanwhile, above 950 mb, a general increase of 10° – 20° in the rms error occurs between 3 and 10 h (Fig. 8). The rms error remains nearly the same until 22 h, except for an additional increase between 400 and 600 mb. With the exception of a lower-tropospheric positive bias during the afternoon hours, the wind speed errors did not exhibit any appreciable biases at upper levels (not shown).

b. Regime classification during 2000

1) SURFACE WIND REGIME

Table 2 summarizes the total number of days for the 0000 and 1200 UTC forecast cycles that were classified into the onshore (easterly), offshore (westerly), and light wind regimes. The 1200 UTC forecast cycle temperature errors under each surface wind regime are shown in Fig. 9. The offshore flow regime tends to yield higher predicted daytime temperatures in RAMS as is evident by the mean temperature plots in Fig. 9a. Among the three surface wind regimes, the light wind regime experiences the largest rms error (not shown) and cold bias during the afternoon and evening hours (6–12 h in Fig. 9b).

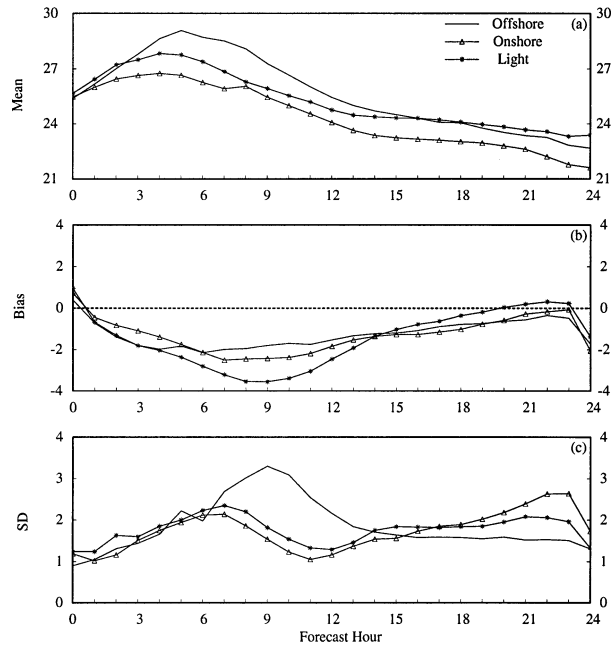


FIG. 9. A plot of the 1200 UTC RAMS temperature errors ($^{\circ}$ C) during offshore (solid line), onshore (triangles), and light surface wind regimes (asterisks) for the 2000 FL warm season. The temperature is verified at the 1.8-m level of the KSC/CCAFS wind tower network. Parameters plotted as a function of forecast hour are (a) mean forecast temperature under each wind regime, (b) bias, and (c) error standard deviation (SD).

The onshore and light wind regimes have a nearly identical pattern of random errors given by the SD in Fig. 9c; however, the random portion of the offshore wind regime errors are substantially larger than the other two wind regimes during the late afternoon and evening hours. It is interesting to note that the smallest daytime bias occurs with the offshore wind regime as well. This larger random error during offshore surface winds is likely the result of an increased occurrence of convection in the vicinity of KSC/CCAFS under this flow regime. Depending on the strength, westerly low-level flow maintains the ECSB boundary near KSC/CCAFS, providing a focusing mechanism for afternoon and evening convection (López and Holle 1987). This convection can subsequently produce significant outflow boundaries resulting in localized temperature gradients and large errors between the RAMS-predicted and observed wind tower temperatures.

The results of the wind regime classification also reveal two very apparent characteristics of the wind direction errors. First, the offshore wind regime contains the largest rms error during the afternoon and evening hours (50° – 70° between 6 and 12 h), likely associated with the higher frequency of convection under surface westerly flow (Fig. 10a). Second, the light wind regime is the primary contributor to the large rms errors during the late night and early morning hours, as expected. Under surface offshore wind flow, the 1200 UTC wind

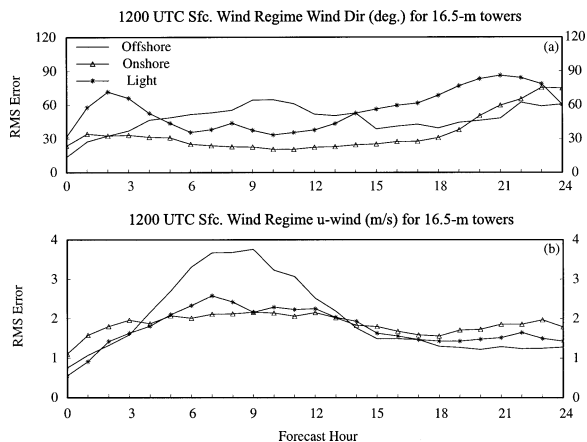


FIG. 10. A plot of the 1200 UTC RAMS wind errors during offshore (solid line), onshore (triangles), and light surface wind regimes (asterisks) for the 2000 FL warm season. Parameters plotted as a function of forecast hour are (a) wind direction rms error ($^{\circ}$) and (b) u -wind component rms error ($m s^{-1}$). The winds are verified at the 16.5-m level of the KSC/CCAFS wind tower network.

direction rms errors reach a maximum of 60° – 70° between 2100 and 2300 UTC (9–11 h in Fig. 10a). Meanwhile, the rms errors associated with onshore wind flows are less than 30° between 1800 and 0300 UTC (6–15 h). The afternoon and evening rms errors in light wind regimes (30° – 50° from 6 to 15 h) range between those of offshore and onshore wind flows.

The largest 1200 UTC wind direction rms errors are associated with the light winds that occur between 0–3 and 18–24 h (Fig. 10a). The rms error grows substantially from 30° to 70° in the first two forecast hours of the light wind regime (Fig. 10a) before tapering as mean wind speeds increase markedly during the day (not shown). The maximum rms error under light winds ($\sim 90^{\circ}$) occurs during the late night hours at 0900 UTC (21 h). These results illustrate how the variable nature of light winds leads to very large errors in wind direction; however, as wind speeds approach zero, the wind direction errors must be used with caution. In these instances, an examination of the individual wind component errors is helpful to determine the representative magnitude of the wind errors. The u -wind rms errors in Fig. 10b are by far the largest under offshore flow during the afternoon and evening hours (6–12 h) and smallest under onshore and light flow. Note that the u -wind rms errors under light winds do not exhibit the distinct maxima as in the wind direction errors of Fig. 10a. Similar results occurred in the RAMS 0000 UTC forecast cycle.

2) THUNDERSTORM DAY REGIME

The most significant characteristic of the temperature errors associated with different thunderstorm-day regimes is that the random errors are largest during the afternoon and evening hours (2° – $3^{\circ}C$) when thunderstorms were observed. In general, the SD is uniform

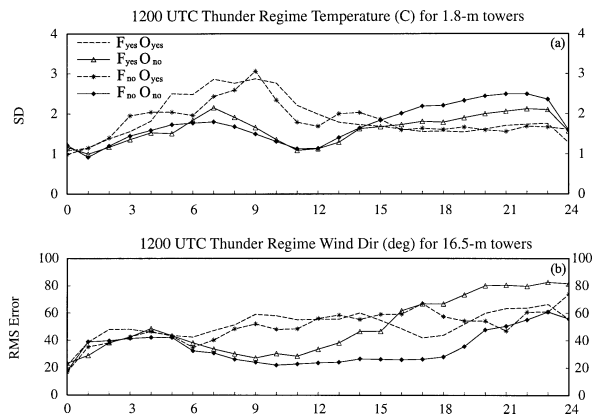


FIG. 11. A plot of 1200 UTC RAMS temperature and wind direction errors for the four contingency combinations of thunderstorm forecasts ($F_{yes}O_{yes}$, $F_{yes}O_{no}$, $F_{no}O_{yes}$, $F_{no}O_{no}$) where F stands for forecast and O for observed during the 2000 FL warm season. Parameters plotted as a function of forecast hour are (a) temperature error standard deviation (SD, $^{\circ}C$), and (b) wind direction rms error ($^{\circ}$). The temperatures are verified at the 1.8-m level of the KSC/CCAFS wind tower network whereas the wind directions are verified at 16.5 m. Dashed lines indicate observed thunderstorm contingencies.

when thunderstorms were not observed ($F_{yes}O_{no}$ and $F_{no}O_{no}$ plots in Fig. 11a, based on Table 3), ranging from 1° to $2^{\circ}C$ for most forecast hours. However, the random forecast errors approach $3^{\circ}C$ between 6 and 12 h during the days when thunderstorms were observed ($F_{yes}O_{yes}$ and $F_{no}O_{yes}$ plots in Fig. 11a). These results indicate that observed thunderstorms and associated outflow boundaries appear to have the greatest impact on the random component of the forecast temperature errors in the 1200 UTC cycle, regardless of whether RAMS predicted any thunderstorms.

A distinct segregation of errors for observed versus no observed thunderstorm days is also evident in the wind direction rms error field for the 1200 UTC forecast cycle. During the afternoon and evening hours (6–12 h), the wind direction rms error increases dramatically when thunderstorms were observed ($F_{yes}O_{yes}$ and $F_{no}O_{yes}$ plots in Fig. 11b). In contrast, the rms error decreases during the same forecast hours on days when thunderstorms were not observed ($F_{yes}O_{no}$ and $F_{no}O_{no}$ plots of Fig. 11b). Since the wind direction biases are negligible in comparison with the rms error (not shown), these results suggest that observed thunderstorms are significant contributors to random wind direction errors during the afternoon and evening hours, regardless of whether RAMS predicted any thunderstorms. The 0000 UTC cycle results did not show such a distinct error pattern, possibly because of the overall poorer performance in thunderstorm prediction (see section 5b).

c. Comparison between RAMS and the Eta Model at TTS

The RAMS and Eta temperature errors for the 2000 warm season are shown in Fig. 12. With the exception

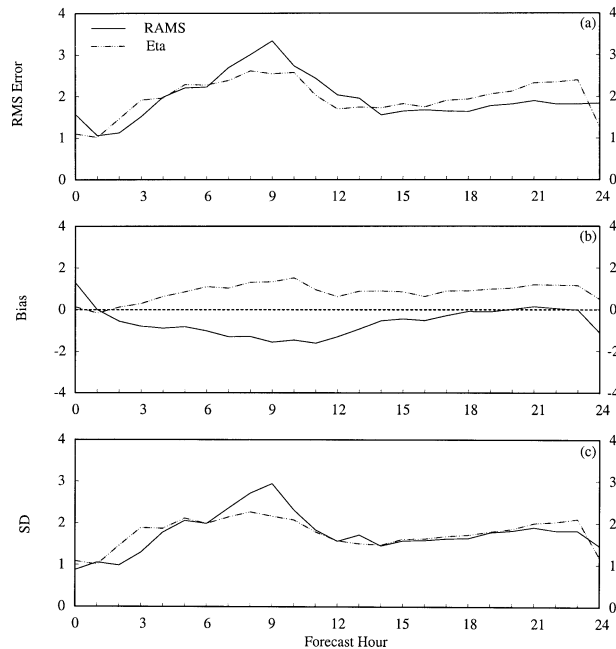


FIG. 12. A comparison between the 1200 UTC forecast cycle surface temperature errors ($^{\circ}\text{C}$) from the RAMS operational configuration and the Eta Model during the 2000 FL warm season. Surface temperatures are verified at TTS only (refer to Fig. 1 for TTS location). Parameters plotted as a function of forecast hour are (a) rms error, (b) bias, and (c) error standard deviation (SD). The plotting convention is a solid line for the RAMS forecasts and a dotted-dashed line for the Eta Model.

of a few minor deviations, the temperature rms errors are within 0.5°C of one another for all forecast hours (Fig. 12a). The total errors of both models are composed of a warm bias up to 1.5°C in the Eta Model and a cold bias approaching -2°C in RAMS (Fig. 12b). The random errors given by the SD plots in Fig. 12c are nearly identical, especially after the 10-h forecast. For dewpoint, RAMS has a slight advantage over the Eta Model during most forecast hours. RAMS generally has about a 0.5°C smaller rms error than the Eta Model (not shown) because the Eta Model experiences a larger moist bias than RAMS, especially during the nocturnal hours.

The wind direction rms error and bias are given in Fig. 13. Between 0 and 1 h, RAMS has a smaller rms error because of the model initialization using local data; however, this error grows to that of the Eta Model by the 2-h forecast (Fig. 13a). Between 6 and 15 h, the RAMS rms errors are about 5° – 15° larger than the Eta and thereafter the errors are comparable. In Fig. 13b, the biases for both models are negligible relative to the magnitude of the rms error. Based on these objective results, it appears as if the high-resolution RAMS configuration does not offer much improvement over the Eta Model; however, this comparison was performed only at a single Eta point forecast location. Since the raw Eta forecast grids were not archived in real time

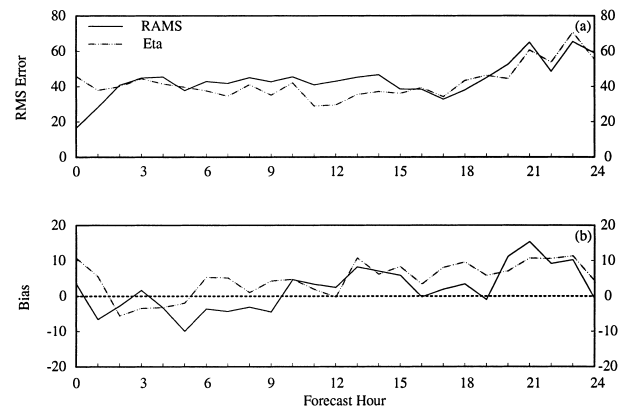


FIG. 13. A comparison between the 1200 UTC forecast cycle surface wind direction errors ($^{\circ}$) from the RAMS operational configuration and the Eta Model during the 2000 FL warm season. Surface wind direction is verified at TTS only. Parameters plotted as a function of forecast hour are (a) rms error and (b) bias. The plotting convention is a solid line for the RAMS errors and a dotted-dashed line for the Eta Model errors.

for interpolation to various local observational sensors, the objective statistics do not account for the spatial variations within the grid forecasts. The subjective sea-breeze evaluation results in the next section will highlight the skill improvements of RAMS over the Eta Model when predicting the sea-breeze phenomenon.

5. Subjective verification results

The AMU conducted an extensive sea-breeze verification for the 1999 and 2000 Florida warm seasons to determine the potential utility of RAMS for surface wind forecast guidance during the warm season. In addition, the AMU benchmarked the skill of RAMS sea-breeze predictions against the NCEP Eta Model point forecasts at TTS and compared the skill of the operational RAMS configuration with the coarser three-grid configuration of RAMS. Furthermore, the AMU conducted a thunderstorm initiation verification during the 2000 warm season months. This section presents the results from the sea-breeze verification during the 1999 and 2000 summer months, as well as the thunderstorm initiation verification from May to September 2000.

a. Sea-breeze verification

1) FOUR-GRID RESULTS FOR 1999 AND 2000 WARM SEASONS

Tables 4 and 5 show a contingency table and categorical and skill scores for the occurrence of a sea-breeze passage at the 12 selected KSC/CAFS towers during the 1999 and 2000 warm seasons. These tables represent 9 months of data (May–August 1999 and May–September 2000) for both the 0000 and 1200 UTC RAMS forecast cycles. If no data were missing, the theoretical maximum number of elements in Table 4

TABLE 4. Contingency tables of the occurrence of the operational RAMS forecast vs observed sea breeze, verified at each of the 12 selected KSC/CCAFS towers during the 1999 and 2000 FL warm seasons.

	Observed sea breeze	No observed sea breeze
0000 UTC forecast cycle		
Forecast sea breeze	1381	261
No forecast sea breeze	228	599
1200 UTC forecast cycle		
Forecast sea breeze	1575	293
No forecast sea breeze	34	567

would be 3312 for each forecast cycle (276 days multiplied by 12 wind towers); however, several forecasts were missing and several towers experienced various outages, particularly during the 2000 warm season. In addition, when either the 0000 or 1200 UTC forecast was missing on a given day, the other forecast cycle was removed to maintain the exact same database for statistical comparison between the two forecast cycles. As a result, about 75% (2469 elements) of the possible data are available for the overall sea-breeze evaluation.

Based on the results in Tables 4 and 5, observed sea-breeze passages occurred at the 12 wind towers about 65% of the time (1609 out of 2469 elements), of which RAMS correctly predicted 86% of them in the 0000 UTC cycle and 98% of them in the 1200 UTC cycle, according to the POD in Table 5. The probability of a null event (PON, not shown), the score analogous to POD for correct “no” forecasts of a sea breeze, indicates that both forecast cycles correctly predict non-sea-breeze days only 66%–70% of the time. The FAR is 16% for both the 0000 and 1200 UTC RAMS cycles. As a result of the higher POD in the 1200 UTC forecasts, this forecast cycle has the highest CSI and HSS. The HSS of 0.69 indicates that RAMS demonstrates a significant amount of utility in predicting the occurrence of the sea breeze. By applying statistical significance tests following the methodology used in Hamill (1999), each of the differences in scores between the 0000 and 1200 UTC forecasts was determined to be statistically significant at the 99% confidence level, except for the FAR (refer to Table A1 in the appendix). It is hypothesized that the 1200 UTC cycle outperformed the 0000 UTC cycle because of the grid-3 boundary conditions overwhelming the 0000 UTC cycle’s local forcing leading up to the sea-breeze onset. An expansion of the innermost grid combined with a shorter integration time may help to alleviate the boundary condition problems as discussed in Warner et al. (1997).

In the instances when RAMS correctly forecast a sea-breeze occurrence, the timing errors were determined at each of the wind towers during the 9-month evaluation period. Table 6 summarizes the timing error statistics for all the correct sea-breeze forecasts for both the 0000 and 1200 UTC cycles. In general, the rms error ranges from 1.5 to 2.1 h for each category of wind towers. The

TABLE 5. Categorical and skill scores of RAMS forecast vs observed sea breeze during the 1999 and 2000 FL warm seasons derived from the contingency tables in Table 4.

Parameter	0000 UTC forecast cycle	1200 UTC forecast cycle
Probability of detection	0.86	0.98
False alarm rate	0.16	0.16
Bias	1.02	1.16
Critical success index	0.74	0.83
Heidke skill score	0.56	0.69

errors are smallest at the coastal towers and largest at the mainland towers, but the variation between these locations is less than 0.5 h, which is smaller than the data sampling rate of once per hour. In all instances the bias is -0.2 or -0.3 h, which is negligible in comparison with the sampling rate.

2) COMPARISON BETWEEN FOUR-GRID AND THREE-GRID DURING 2000

In addition to the evaluation of the operational RAMS forecast sea breezes, a sensitivity test was conducted to compare the sea-breeze verification results between the operational RAMS and a coarser RAMS grid configuration during the 2000 warm season (May–September). This sensitivity experiment compared the RAMS four-grid sea-breeze forecasts with RAMS three-grid forecasts, where the innermost 1.25-km grid was simply excluded during the model’s rerun of all forecasts during the 2000 warm season. As a result, the three-grid RAMS configuration has a 5-km horizontal grid spacing over KSC/CCAFS. To generate point forecasts from the three-grid RAMS, the gridded forecasts from the 5-km grid were interpolated to the sensor locations in the same manner as described in section 3. The sea-breeze verification was then conducted at the 12 selected wind towers (Fig. 2a) for all common four-grid and three-grid RAMS forecasts utilizing the same onshore versus offshore criteria at each wind tower.

According to Table 7, the four-grid RAMS configuration outperforms the coarser three-grid configuration in virtually all categorical and skill categories. The 0000 UTC POD is 11% higher in the four-grid RAMS when

TABLE 6. A summary of timing error statistics for the May–Aug 1999 and May–Sep 2000 evaluation periods is given for the subjective sea-breeze verification performed for the 12 selected KSC/CCAFS towers. The rms error and bias are shown in units of hours for the 0000 and 1200 UTC forecasts.

Location	Statistic	0000 UTC cycle	1200 UTC cycle
Coastal towers	Rms error	1.8	1.5
	Bias	-0.3	-0.3
Merritt Island towers	Rms error	1.9	1.7
	Bias	-0.3	-0.2
Mainland towers	Rms error	2.1	1.9
	Bias	-0.3	-0.2

TABLE 7. Categorical and skill scores of the 0000 and 1200 UTC RAMS four-grid and three-grid forecast vs observed sea breezes during the 2000 FL warm season.

Parameter	0000 UTC forecast cycle		1200 UTC forecast cycle	
	RAMS four grid	RAMS three grid	RAMS four grid	RAMS three grid
	Probability of detection	0.82	0.71	0.98
False alarm rate	0.17	0.19	0.15	0.15
Bias	0.98	0.88	1.15	1.08
Critical success index	0.70	0.61	0.84	0.79
Heidke skill score	0.54	0.41	0.71	0.64

compared with the three-grid configuration, resulting in an increase in both the CSI and HSS. In addition, the bias is very near unity (i.e., unbiased) in the 0000 UTC four-grid runs whereas the three-grid forecasts have a bias of 0.88 since the coarser resolution runs slightly underforecast the occurrence of the sea breeze (Table 7).

In the 1200 UTC RAMS forecasts, both model configurations improve in the categorical and skill scores except for the bias. The four-grid forecasts continue to outperform the three-grid forecasts in detecting the sea breeze over KSC/CCAFS. The POD improves to 98% in the four-grid configuration and 92% in the three-grid forecasts, whereas the CSI and HSS are 5% and 7% better, respectively, in the four-grid versus three-grid predictions (Table 7). Furthermore, the four westernmost towers over mainland Florida (refer to Fig. 2) exhibited the greatest discrepancy in skill between the four-grid and three-grid RAMS forecasts during the 2000 warm season. The POD is 14% higher in the four-grid forecasts, resulting in a 9% higher CSI and 11% higher HSS (not shown). The 5-km horizontal grid spacing of RAMS grid 3 is not sufficient to resolve the interactions between the river- and sea-breeze circulations adequately since, theoretically, it cannot depict features whose wavelengths are less than 20 km (4 times the horizontal grid spacing). Meanwhile, the 1.25-km grid spacing can resolve features with wavelengths as small as 5 km, which is comparable to the scale of the river- and lagoon-breeze circulations. All of the measured differences except the FAR are statistically significant at the 98% confidence level, indicating that the four-grid configuration is indeed a better forecaster of the sea-breeze occurrences than is the coarser three-grid RAMS configuration.

3) COMPARISON BETWEEN RAMS AND ETA AT TTS DURING 2000

The third and final sea-breeze evaluation compares the operational RAMS with the Eta point forecasts at TTS. For this benchmark, the 13–23-h forecasts from the RAMS and Eta 0000 UTC forecasts, and the 1–11-h forecasts from the 1200 UTC forecasts, are compared.

TABLE 8. Categorical and skill scores of the 0000 and 1200 UTC RAMS and Eta forecast vs observed sea breezes at TTS during the 1999 and 2000 FL warm seasons.

Parameter	0000 UTC forecast cycle		1200 UTC forecast cycle	
	RAMS	Eta	RAMS	Eta
Probability of detection	0.83	0.53	0.92	0.77
False alarm rate	0.15	0.13	0.18	0.09
Bias	0.98	0.61	1.12	0.85
Critical success index	0.72	0.49	0.77	0.71
Heidke skill score	0.61	0.38	0.68	0.65

This technique gives the Eta Model an inherent advantage over RAMS because RAMS is forced by Eta 12–36-h forecasts from the Eta cycle 12 h prior to RAMS initialization. Nonetheless, this analysis will show that despite this advantage for the Eta Model, RAMS still outperforms the Eta Model in predicting the occurrence of the ECSB at TTS. The ideal benchmark would have been to compare the RAMS versus the Eta forecasts, both interpolated to the 12 selected KSC/CCAFS wind towers. This comparison would have illustrated how the 1.25-km RAMS grid can resolve far more spatial variability than the 32-km Eta; however, this analysis could not be performed since the Eta forecast grids were not archived for this study.

Table 8 summarizes the skill comparison between the RAMS and Eta predictions of the ECSB occurrence at TTS during the 1999 and 2000 warm seasons. Note that only 0000 UTC Eta forecasts were available during the four evaluation months in 1999, whereas both the 0000 and 1200 UTC Eta forecasts were available for the five evaluation months of 2000; thus, the sample size is larger for the 0000 UTC cycle. In the 0000 UTC forecasts, RAMS correctly predicted the occurrence of the ECSB at TTS with a much higher percentage than the Eta Model (POD difference of 30% to the advantage of RAMS in Table 8). One advantage of the Eta Model is a better PON at 88% versus 78% in RAMS; however, the higher PON in the Eta Model primarily results from the much lower tendency for it to predict sea breezes (given by the bias of only 0.61 in Table 8). Since the FAR is comparable and the POD is significantly higher in RAMS, the CSI and HSS are much higher in RAMS as well. For the 0000 UTC cycle, all differences in categorical and skill scores are statistically significant at the 99% level except the differences in FAR (refer to Table A1).

Even though RAMS dramatically outperformed the Eta Model during the 0000 UTC forecast cycle, the same cannot be said for the 1200 UTC cycle. RAMS still has a significantly higher POD than the Eta Model; however, RAMS also has a significantly higher FAR. As a result, the CSI and HSS (Table 8) are only marginally better in RAMS. In fact, neither the CSI nor the HSS differences are statistically significant above the 86% confidence interval. In contrast, the higher FAR in RAMS

TABLE 9. A list of the number and percentage of days that RAMS correctly identified one or more of the grid-4 zones for thunderstorm initiation, as well as the number and percentage of days that RAMS correctly predicted thunderstorm initiation to the nearest hour, within ± 1 h, within ± 2 h, and within ± 3 h. The total is based on the number of correctly predicted thunderstorm days.

Parameter	0000 UTC cycle			1200 UTC cycle		
	No.	Total	Percentage correct	No.	Total	Percentage correct
\geq one zone correct	21	36	58	29	63	46
Correct timing	3	36	8	12	63	19
Timing within ± 1 h	13	36	36	26	63	42
Timing within ± 2 h	19	36	53	38	63	61
Timing within ± 3 h	26	36	72	48	63	77

is statistically significant in comparison with the Eta Model, suggesting that RAMS has a tendency to overpredict the occurrence of the ECSB in the 1200 UTC cycle compared to the Eta Model. Overall though, RAMS clearly demonstrates that it has the ability to better detect the occurrence of the ECSB at TTS during the Florida warm season, especially in the 0000 UTC forecast cycle. These results indicate that, despite the comparable objective error statistics between RAMS and the Eta Model, the phenomenological verification of the ECSB improves over the Eta Model when running RAMS at 1.25-km grid spacing.

b. Thunderstorm initiation verification

In general, both forecast cycles are comparable in terms of the spatial accuracy, whereas the 1200 UTC cycle exhibits more favorable results in the occurrence and timing of thunderstorm initiation. Table 9 summarizes the spatial and temporal results of the RAMS forecast thunderstorm initiation for the 0000 and 1200 UTC cycles. Both forecast cycles correctly predicted thunderstorm initiation in one or more zones (see Fig. 2b) about one-half of the time (58% in the 0000 UTC cycle and 46% in the 1200 UTC cycle). The slightly poorer performance of the 1200 UTC cycle could be attributed to the larger sample size of correctly forecast thunderstorm days (63 versus 36). Note that the number of 1200 UTC correctly forecast thunderstorm days in Table 9 (63) does not match the number in Table 3 (72) because only days with successful 0000 and 1200 UTC forecasts were used to generate the error statistics for the thunderstorm initiation verification. This ensures a fair comparison between the 0000 and 1200 UTC thunderstorm forecast skill.

In the timing accuracy, only 8% (19%) of the correctly predicted thunderstorm days experienced an exact initiation time to the nearest hour in the 0000 UTC (1200 UTC) cycle. Meanwhile, RAMS correctly predicted the hourly thunderstorm initiation time within ± 3 h of the observed time on about 75% of all days for both forecast cycles (slightly higher in the 1200 UTC forecasts). The timing rms errors of thunderstorm initiation anywhere

on RAMS grid 4 were generally between 2 and 3 h for both forecast cycles whereas the bias was about +1 h (too late) in the 0000 UTC cycle and 0 h in the 1200 UTC cycle (not shown). The timing error statistics for thunderstorm initiation in each individual grid-4 zone did not exhibit any trends or organized patterns that favored specific zones. Note that these timing errors in RAMS do not reflect off-hour predictions because forecast output was available only at the top of each hour.

Figure 14 shows the POD and FAR scores of the thunderstorm occurrence for both RAMS forecast cycles as a function of grid-4 zone (Fig. 2b) and timing thresholds. In all six zones, the 0000 UTC POD is less than 0.40 under all timing thresholds whereas the FAR is typically larger than the POD (Figs. 14a and 14b), suggesting that the 0000 UTC forecast cycle has limited value in predicting the occurrence of thunderstorms in any zone on grid 4. The 1200 UTC forecast cycle shows marked improvement over the 0000 UTC cycle, since the POD scores are typically higher by a factor of 2 or more (Figs. 14a and 14c). However, the FAR is still quite high, especially when verifying RAMS thunderstorm initiation to the nearest hour ($\text{FAR} > 0.4$ in Fig. 14d). These results indicate that the more recent initialization of RAMS to the time of convection initiation improves the predictions of the occurrence of thunderstorms, but does not considerably improve the accuracy of the predicted location and timing of thunderstorm initiation. Future efforts could involve correlating the thunderstorm forecast errors (both the objective regime classification and subjective results) with the model's tendency to overstabilize the lower troposphere.

This limited skill in the predicted location and timing of thunderstorm initiation could be related to several characteristics of the current RAMS configuration. First, the lateral boundaries of grid 4, particular the eastern boundary, are not sufficiently displaced from the area of interest (e.g., the Florida east coast). Expansion of grid 4 could alleviate the impacts caused by lateral boundary interactions with the coarser grid, especially in zone 6 (Warner et al. 1997). Second, errors in precipitation and the vertical distribution of latent heating, associated with the parameterized treatment of convection on the outer grids, greatly affect the explicit convective forecasts on the inner grid (Warner and Hsu 2000). In fact, Warner and Hsu (2000) found that different precipitation parameterizations on the outer grids produced up to a factor-of-3 difference in their 24-h precipitation forecasts. Third, soil moisture data are not ingested into RAMS nor initialized based on previous rainfall. Horizontal variations in soil moisture resulting from past rainfall events can play an important role in determining the favored locations of convective initiation (Lynn et al. 1998). The combination of ingesting soil moisture observations and running an antecedent precipitation index algorithm using previous rainfall data can result in a more accurate soil moisture initial condition for RAMS. Last, a more sophisticated me-

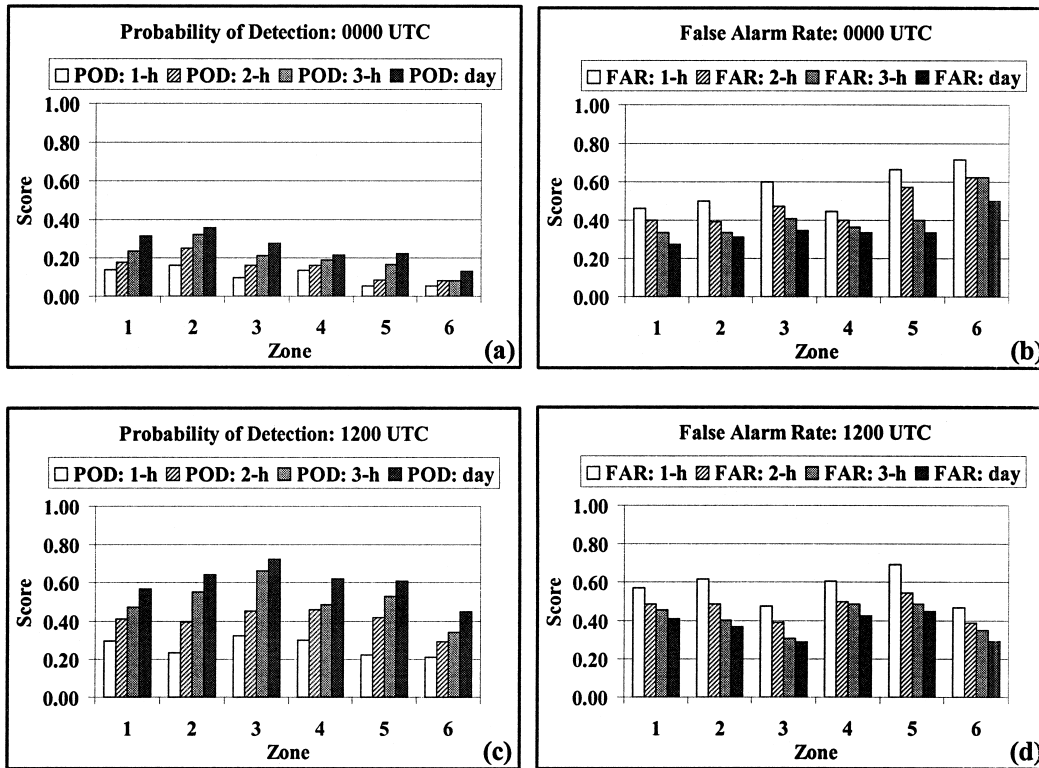


FIG. 14. The POD and FAR for the RAMS 0000 and 1200 UTC forecasts of the first daily thunderstorm occurrence in each zone of grid 4 during the hours of 1500–2300 UTC. The plots shown are (a) 0000 UTC POD, (b) 0000 UTC FAR, (c) 1200 UTC POD, and (d) 1200 UTC FAR. The scores were determined by verifying hourly RAMS thunderstorm occurrences to the nearest 1, 2, and 3 h and for the entire daily verification period according to the scale provided.

soscale data assimilation scheme than the current cold-start initialization is needed for RAMS, where high-resolution, continuous observational data such as from Weather Surveillance Radar-1988 Doppler (WSR-88D) and satellite data are assimilated and brought into balance with the model equations.

6. Summary

This paper presented an objective and subjective evaluation of a real-time, high-resolution configuration of RAMS, as run operationally at CCAFS in east-central Florida. The RAMS forecast output provides input to the HYPACT toxic dispersion model, which serves as guidance to 45 SW/SE personnel during space launch operations at KSC/CAFS. Thus, knowledge of the accuracy of RAMS forecasts is critical in determining the accuracy of results from HYPACT.

Because RAMS is initialized with a cold-start configuration and the analysis may overfit the observations, the model errors grow rapidly within 1–2 h of initialization. The most significant error found in this version of RAMS is a prominent cold bias at the surface and lower troposphere (primarily during the daylight hours), resulting in a vertical temperature profile that is too stable when compared with observations. In general, the

magnitudes of the point error statistics from the objective evaluation do not suggest much improvement of RAMS over the Eta Model; however, point error statistics alone cannot adequately measure the accuracy and utility of high-resolution model forecasts. A subjective verification of specific meteorological phenomena is required to provide an appropriate measure of the model's added value.

Based on the results of the subjective verification, the 1.25-km RAMS grid has the greatest skill in predicting the Florida ECSB when compared with the 5-km RAMS and the Eta Model. These 1.25-km RAMS sea-breeze forecasts are significantly more skillful than 5-km RAMS forecasts, as well as the 0000 UTC cycle of the Eta Model at TTS. Despite the accurate sea-breeze forecasts, RAMS had difficulty in explicitly predicting the time and location of thunderstorm initiation on the 1.25-km grid during the 2000 summer months. This difficulty could result from the cold-start initialization, boundary condition problems, erroneous interactions from the cumulus parameterization on the coarser grids, and/or an inadequate data integration and assimilation scheme in the current configuration.

Future efforts to support weather forecasting and toxic dispersion modeling at KSC/CAFS include an implementation of the fifth-generation Pennsylvania State

University–National Center for Atmospheric Research Mesoscale Model (MM5) at the Eastern Range through the Range Standardization and Automation program. A configuration of MM5 comparable to the current RAMS configuration will be run operationally at CCAFS using the Local Analysis and Prediction System to assimilate and analyze high-resolution observational data. The LAPS analyses will be cycled with the MM5 forecasts to improve data assimilation and reduce the model’s initial error growth. The result should be further improvements in high-resolution NWP over east-central Florida in support of the U.S. space program.

Acknowledgments. The authors thank Dr. Frank Mercet for his internal review of the manuscript. The authors also appreciate the constructive comments from three anonymous reviewers who helped to improve the quality of the paper.

Mention of a copyrighted, trademarked, or proprietary product, service, or document does not constitute endorsement thereof by the authors; ENSCO, Inc.; the AMU; the National Aeronautics and Space Administration; or the U.S. government. Any such mention is solely for the purpose of fully informing the reader of the resources used to conduct the work reported herein.

APPENDIX

Determining the Statistical Significance of Model Skill Scores Differences

The AMU used a resampling methodology (Wilks 1995; Hamill 1999) to determine the levels of statistical significance in the differences between the POD, FAR, CSI, HSS, and bias. Resampling involves randomly shuffling the daily sea-breeze verification of one model or configuration versus the other. This random shuffling is performed many times to obtain a sufficient database. The null hypothesis for this test is that the differences between the categorical or skill scores (S) is zero,

$$H_0: S_1 - S_2 = 0.0, \tag{A1}$$

and the alternative hypothesis is that the difference is not equal to zero,

$$H_A: S_1 - S_2 \neq 0.0. \tag{A2}$$

Assume a two-sided test with a significance level $\alpha = 0.05$. The test statistic and resampled distribution are formed based on this null hypothesis.

The contingency tables for the comparisons of the operational RAMS 0000 UTC versus 1200 UTC forecast cycles and the RAMS four-/three-grid configurations were developed from daily verifications at the 12 selected KSC/CCAFS wind towers. On a given day, it is likely that the forecast sea-breeze occurrences at the 12 wind towers experience a spatial correlation. Therefore, the resampling methodology handles this correlation by grouping the total contingency table elements for each

day into a vector array of size n , the number of days during the evaluation:

$$\mathbf{x}_{i,j} = (a, b, c, d)_{i,j}, \quad i = 1, 2, \quad \text{and} \\ j = 1, \dots, n, \tag{A3}$$

where i is the model indicator (e.g., RAMS or Eta), j is the number of the individual day, and (a, b, c, d) represent the four elements of the 2×2 contingency table. The test statistic is simply the actual difference in the skill score as computed from the overall contingency table results:

$$(\hat{S}_1 - \hat{S}_2) = (a, b, c, d)_1 - (a, b, c, d)_2 \\ = \sum_{k=1}^n \mathbf{x}_{1,k} - \sum_{k=1}^n \mathbf{x}_{2,k}. \tag{A4}$$

To build a resampled distribution and test the null hypothesis, a random number generator is used to pick either one model (configuration) or the other on each day ($1, \dots, n$) from the two vector arrays. After the first resampled distribution is generated by this method, a second distribution is constructed using the model (configuration) data not selected in the first distribution. These two resampled arrays are each summed to form two new sets of contingency table elements. The categorical and skill scores are calculated for these two contingency tables and the differences in the scores are computed:

$$(\hat{S}_1^* - \hat{S}_2^*) = (a, b, c, d)_1^* - (a, b, c, d)_2^* \\ = \sum_{k=1}^n \mathbf{x}_{I_k,k} - \sum_{k=1}^n \mathbf{x}_{(3-I_k),k}, \tag{A5}$$

where I_k is a random number indicator equally likely to take on the value 1 or 2 (one model or the other). This process of resampling is repeated 10 000 times to build the null distribution.

The hypothesis of the differences in skill scores is tested by identifying the location of the actual differences in skill scores, $(\hat{S}_1 - \hat{S}_2)$, in the resampled distribution, $(\hat{S}_1^* - \hat{S}_2^*)$. The net result of the resampling distribution is to compute the numbers \hat{t}_L and \hat{t}_V such that

$$P^*[(\hat{S}_1^* - \hat{S}_2^*) < \hat{t}_L] = \frac{\alpha}{2} = 0.025, \quad \text{and} \tag{A6}$$

$$P^*[(\hat{S}_1^* - \hat{S}_2^*) > \hat{t}_V] = 1 - \frac{\alpha}{2} = 0.975,$$

where P^* represents probabilities calculated from the resampled distribution. The null hypothesis, H_0 , is rejected if $(\hat{S}_1 - \hat{S}_2) < \hat{t}_L$ or $(\hat{S}_1 - \hat{S}_2) > \hat{t}_V$. The results of this resampling method are shown in Table A1 for most individual categorical and skill scores presented. Each column in Table A1 represents a significance test by subtracting one forecast or configuration from another. If the test statistic is greater than 97.5%,

TABLE A1. Levels of statistical significance (%) for various comparisons of the RAMS and Eta sea-breeze categorical and skill scores using a two-tailed, resampling method following Hamill (1999). The RAMS-vs-Eta tests are valid for the sea-breeze evaluation at TTS while the comparison of different configurations and initializations of RAMS are valid at the 12 KSC/CCAFS wind towers in Fig. 2a. Scores that are statistically significant at 95% confidence or higher are highlighted in bold italic font.

Parameter	RAMS 1200 UTC minus 0000 UTC	RAMS four-grid minus three- grid (0000 UTC)	RAMS four-grid minus three- grid (1200 UTC)	RAMS minus Eta (0000 UTC)	RAMS minus Eta (1200 UTC)
POD	100%	99.9%	99.9%	100%	99.9%
FAR	46.2%	14.9%	35.0%	66.5%	98.1%
Bias	100%	98.5%	99.6%	100%	100%
CSI	100%	99.9%	99.2%	99.9%	86.1%
HSS	99.6%	99.4%	96.3%	99.2%	58.3%

then the skill of forecast 1 is significantly higher than that of forecast 2. Conversely, if the test statistic is less than 2.5%, then the skill of forecast 2 is significantly higher than that of forecast 1.

REFERENCES

- Benjamin, S. G., J. M. Brown, K. J. Brundage, B. Schwartz, T. Smirnova, T. L. Smith, L. L. Morone, and G. J. DiMego, 1998: The operational RUC-2. Preprints, *16th Conf. on Weather Analysis and Forecasting*, Phoenix, AZ, Amer. Meteor. Soc., 249–252.
- Bringi, V. N., K. Knupp, A. Detwiler, L. Liu, I. J. Caylor, and R. A. Black, 1997: Evolution of a Florida thunderstorm during the Convection and Precipitation/Electrification Experiment: The case of 9 August 1991. *Mon. Wea. Rev.*, **125**, 2131–2160.
- Case, J., 2000: Interim report on the evaluation of the Regional Atmospheric Modeling System in the Eastern Range Dispersion Assessment System. NASA Contractor Rep. CR-2000-208576, Kennedy Space Center, FL, 102 pp. [Available from ENSCO, Inc., 1980 N. Atlantic Ave., Suite 230, Cocoa Beach, FL 32931.]
- , 2001: Final report on the evaluation of the Regional Atmospheric Modeling System in the Eastern Range Dispersion Assessment System. NASA Contractor Rep. CR-2001-210259, Kennedy Space Center, FL, 147 pp. [Available from ENSCO, Inc., 1980 N. Atlantic Ave., Suite 230, Cocoa Beach, FL 32931.]
- Cetola, J. D., 1997: A climatology of the sea breeze at Cape Canaveral, Florida. M.S. thesis, Dept. of Meteorology, The Florida State University, Tallahassee, FL, 56 pp.
- Chen, S., and W. R. Cotton, 1988: The sensitivity of a simulated extratropical mesoscale convective system to longwave radiation and ice-phase microphysics. *J. Atmos. Sci.*, **45**, 3897–3910.
- Chuang, H.-Y., and G. Manikin, cited 2002: The NCEP Meso-Eta post processor: A documentation. [Available online at <http://www.emc.ncep.noaa.gov/mmb/papers/chuang/1/OF438.html>.]
- Cotton, W. R., M. A. Stephens, T. Neuhoff, and G. J. Tripoli, 1982: The Colorado State University three-dimensional cloud/mesoscale model—1982. Part II: An ice phase parameterization. *J. Rech. Atmos.*, **16**, 295–320.
- Davies, H. C., 1983: Limitations of some common lateral boundary schemes used in regional NWP models. *Mon. Wea. Rev.*, **111**, 1002–1012.
- Doswell, C. A., R. Davies-Jones, and D. Keller, 1990: On summary measures of skill in rare event forecasting based on contingency tables. *Wea. Forecasting*, **5**, 576–585.
- Ernst, J. A., and F. J. Merceret, 1995: The Applied Meteorology Unit: A tri-agency applications development facility supporting the space shuttle. Preprints, *Sixth Conf. on Aviation Weather Systems*, Dallas, TX, Amer. Meteor. Soc., 266–269.
- Evans, R. J., 1996: Final report on the evaluation of the Emergency Response Dose Assessment System (ERDAS). NASA Contractor Rep. CR-201353, Kennedy Space Center, FL, 184 pp. [Available from ENSCO Inc., 1980 N. Atlantic Ave., Suite 230, Cocoa Beach, FL 32931.]
- Hamill, T. M., 1999: Hypothesis tests for evaluating numerical precipitation forecasts. *Wea. Forecasting*, **14**, 155–167.
- Harms, D. E., B. F. Boyd, R. M. Lucci, M. S. Hinson, and M. W. Maier, 1997: Systems used to evaluate the natural and triggered lightning threat to the Eastern Range and Kennedy Space Center. Preprints, *28th Conf. on Radar Meteorology*, Austin, TX, Amer. Meteor. Soc., 240–241.
- Lericos, T. P., H. E. Fuelberg, A. I. Watson, and R. L. Holle, 2002: Warm season lightning distributions over the Florida peninsula as related to synoptic patterns. *Wea. Forecasting*, **17**, 83–98.
- López, R. E., and R. L. Holle, 1987: Distribution of summertime lightning as a function of low-level wind flow in central Florida. Tech. Memo. ESG-28, NOAA/Environmental Research Labs, Boulder, CO, 43 pp.
- Lynn, B. H., W.-K. Tao, and P. J. Wetzel, 1998: A study of landscape-generated deep moist convection. *Mon. Wea. Rev.*, **126**, 928–942.
- Lyons, W. A., and Coauthors, 1993: An interactive operational emergency response dispersion system using a mesoscale numerical prognostic model. Preprints, *Ninth Int. Conf. on Interactive Information and Processing Systems*, Anaheim, CA, Amer. Meteor. Soc., 242–247.
- Manobianco, J., and P. A. Nutter, 1999: Evaluation of the 29-km Eta Model. Part II: Subjective verification over Florida. *Wea. Forecasting*, **14**, 18–37.
- McQueen, J. T., R. A. Valigura, and B. J. B. Stunder, 1997: Evaluation of the RAMS model for estimating turbulent fluxes over the Chesapeake Bay. *Atmos. Environ.*, **31**, 3803–3819.
- Mellor, G. L., and T. Yamada, 1982: Development of a turbulence closure model for geophysical fluid problems. *Rev. Geophys. Space Phys.*, **20**, 851–875.
- Mohanty, U. C., A. Kasahara, and R. Errico, 1986: The impact of diabatic heating on the initialization of divergent circulations in a global forecast model. *J. Meteor. Soc. Japan*, **64**, 805–817.
- Murphy, A. H., 1988: Skill scores based on the mean square error and their relationships to the correlation coefficient. *Mon. Wea. Rev.*, **116**, 2417–2424.
- Nutter, P. A., and J. Manobianco, 1999: Evaluation of the 29-km Eta Model. Part I: Objective verification at three selected stations. *Wea. Forecasting*, **14**, 5–17.
- Pielke, R. A., and Coauthors, 1992: A comprehensive meteorological modeling system—RAMS. *Meteor. Atmos. Phys.*, **49**, 69–91.
- Powell, M. D., and S. K. Rinard, 1998: Marine forecasting at the 1996 centennial Olympic Games. *Wea. Forecasting*, **13**, 764–782.
- Reap, R. M., 1994: Analysis and prediction of lightning strike distributions associated with synoptic map types over Florida. *Mon. Wea. Rev.*, **122**, 1698–1715.
- Salvador, R., J. Calbó, and M. Millán, 1999: Horizontal grid size selection and its influence on mesoscale model simulations. *J. Appl. Meteor.*, **38**, 1311–1329.
- Schaefer, J. T., 1990: The critical success index as an indicator of warning skill. *Wea. Forecasting*, **5**, 570–575.
- Snook, J. S., J. M. Cram, and J. M. Schmidt, 1995: LAPS/RAMS:

- A nonhydrostatic mesoscale numerical modeling system configured for operational use. *Tellus*, **47A**, 864–875.
- , P. A. Stamus, J. Edwards, Z. Christidis, and J. A. McGinley, 1998: Local-domain analysis and forecast model support for the 1996 centennial Olympic Games. *Wea. Forecasting*, **13**, 138–150.
- Takano, I., and A. Segami, 1993: Assimilation and initialization of a mesoscale model for improved spin-up of precipitation. *J. Meteor. Soc. Japan*, **71**, 377–391.
- Tremback, C. J., 1990: Numerical simulation of a mesoscale convective complex: Model development and numerical results. Ph.D. dissertation, Atmospheric Science Paper 465, Colorado State University, Fort Collins, CO, 247 pp.
- , and R. Kessler, 1985: A surface temperature and moisture parameterization for use in mesoscale numerical models. Preprints, *Seventh Conf. on Numerical Weather Prediction*, Montreal, QC, Canada, Amer. Meteor. Soc., 355–358.
- , I. T. Baker, M. Uliasz, and R. F. A. Hertenstein, 1998: Time domain reflectometry of soil moisture for initialization of prognostic mesoscale models. Mission Research Corporation Contract NAS10-12264 for Kennedy Space Center, FL, 339 pp. [Available from ATMET, P.O. Box 19195, Boulder, CO 80308-9195.]
- , R. L. Walko, and M. J. Bell, cited 2002: RAMS/HYPACT Evaluation and Visualization Utilities (REU) user's guide, version 2.3.1. [Available online at <http://www.atmet.com/html/docs/revu/2.3.1/revu Ug-2.3.1.htm>.]
- Turner, D. B., 1986: Comparison of three methods for calculating the standard deviation of the wind direction. *J. Climate Appl. Meteor.*, **25**, 703–707.
- Walko, R. L., C. J. Tremback, and M. J. Bell, cited 2001: Hybrid particle and concentration transport model (HYPACT) user's guide, version 1.2.0. [Available online at <http://www.atmet.com/html/docs/hypact/1.2.0/hypact.htm>.]
- Warner, T. T., and H.-M. Hsu, 2000: Nested-model simulation of moist convection: The impact of coarse-grid parameterized convection on fine-grid resolved convection. *Mon. Wea. Rev.*, **128**, 2211–2231.
- , R. A. Peterson, and R. E. Treadon, 1997: A tutorial on lateral boundary conditions as a basic and potentially serious limitation to regional numerical weather prediction. *Bull. Amer. Meteor. Soc.*, **78**, 2599–2617.
- Wilks, D. S., 1995: *Statistical Methods in the Atmospheric Sciences*. Academic Press, 467 pp.
- Yuter, S. E., and R. A. Houze Jr., 1995a: Three-dimensional kinematic and microphysical evolution of Florida cumulonimbus. Part I: Spatial distribution of updrafts, downdrafts, and precipitation. *Mon. Wea. Rev.*, **123**, 1921–1940.
- and — 1995b: Three-dimensional kinematic and microphysical evolution of Florida cumulonimbus. Part II: Frequency distributions of vertical velocity, reflectivity, and differential reflectivity. *Mon. Wea. Rev.*, **123**, 1941–1963.